ACS Partner Journal

ENVIRONMENT & HEALTH

Open Access

pubs.acs.org/EnvHealth

Article

Oxidation Mechanism and Toxicity Evolution of Linalool, a Typical Indoor Volatile Chemical Product

Published as part of Environment & Health virtual special issue "Grand Environmental Challenge: Indoor Air Pollution, Health Effects, and Mitigation".

Zihao Fu, Song Guo,* Ying Yu, Hong-Bin Xie,* Shiyu Li, Daqi Lv, Putian Zhou, Kai Song, Zheng Chen, Rui Tan, Kun Hu, Ruizhe Shen, Maosheng Yao, and Min Hu

Cite This: *Environ. Health* 2024, 2, 486−498

Read Online

ACCESS | Metrics & More | Article Recommendations | Supporting Information

ABSTRACT: Linalool, a high-reactivity volatile chemical product (VCP) commonly found in cleaning products and disinfectants, is increasingly recognized as an emerging contaminant, especially in indoor air. Understanding the gas-phase oxidation mechanism of linalool is crucial for assessing its impact on atmospheric chemistry and human health. Using quantum chemical calculations and computational toxicology simulations, we investigated the atmospheric transformation and toxicity evolution of linalool under low and high $NO/HO_2\cdot$ levels, representing indoor and outdoor environments. Our findings reveal that linalool can undergo the novel mechanisms involving concerted peroxy ($RO_2\cdot$) and alkoxy radical ($RO\cdot$) modulated autoxidation, particularly emphasizing the importance of cyclization reactions indoors. This expands the widely known $RO_2\cdot$-dominated H-shift-driven autoxidation and proposes a generalized autoxidation mechanism that leads to the formation of low-volatility secondary organic aerosol (SOA) precursors. Toxicological analysis shows that over half of transformation products (TPs) exhibited higher carcinogenicity and respiratory toxicity compared to linalool. We also propose time-dependent toxic effects of TPs to assess their long-term toxicity. Our results indicate that the strong indoor emission coupled with slow consumption rates lead to significant health risks under an indoor environment. The results highlight complex indoor air chemistry and health concerns regarding persistent toxic products during indoor cleaning, which involves the use of linalool or other VCPs.

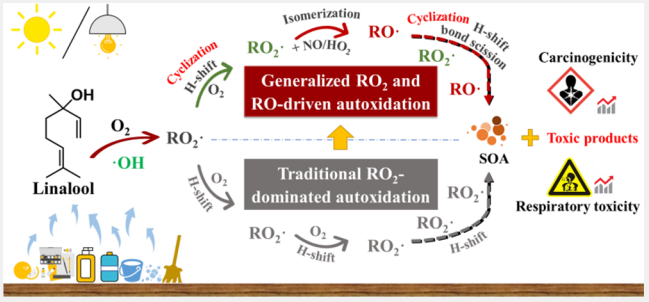

KEYWORDS: *volatile chemical products (VCPs), peroxy radicals ($RO_2\cdot$), atmospheric autoxidation, secondary organic aerosol (SOA), computational toxicology*

1. INTRODUCTION

With the rising demand for chemical products, their environmental transformation and adverse health impacts have emerged as a significant global concern nowadays.[1−3] Due to their potential persistence, bioaccumulation, and toxicity (PBT characteristics), some chemicals cause hazards to environmental and human health, to be defined as the contaminants of emerging concern (CECs).[4,5] Recently, the production and use of volatile chemical products (VCPs, e.g. personal care products, cleaning agents, coatings, adhesives, etc.) has been recognized as a potential source of CECs in not only an indoor environment but also an urban atmosphere.[6−10] However, their emission inventories are not readily available, resulting in a poor understanding of their environmental impacts, which makes it more difficult to sufficiently control and restrict VCPs.[11−13] Considering a large amount of volatile and semi/intermediate volatile compound emissions, VCPs exhibit elevated atmospheric concentrations, thus most likely contributing to the formation of secondary organic aerosol (SOA) and toxic products through atmospheric oxidation, posing greater exposure risks.[6,14−17] In order to understand and assess the role of VCPs in atmospheric chemistry, it is important not only to quantify their emissions but also, more importantly, to understand their atmospheric transformation mechanisms and reactivity.

Linalool (3,7-dimethylocta-1,6-dien-3-ol, $C_{10}H_{18}O$) is an important high-production VCP that is widely used in cosmetics, personal-care, and laundry products.[18−22] The global market size of linalool was valued at US$ 607.06 Mn.

Received: February 14, 2024
Revised: March 21, 2024
Accepted: March 21, 2024
Published: April 2, 2024

https://doi.org/10.1021/envhealth.4c00033
Environ. Health 2024, 2, 486−498

in 2022, and the total linalool revenue is expected to grow by 4.2% from 2023 to 2029.[23] It has been found that anthropogenic linalool contributes a larger fraction of indoor VOC emissions than outdoor emissions; nevertheless, linalool has natural source emissions.[24−27] Recent studies have shown that linalool and oxidized linalool could have a large harmful impact on humans, especially the contact allergy.[20] Therefore, concern about the environmental impact of linalool has been increasing.

It is urgent to assess the environmental risk of linalool to understand its potential environmental and health impacts. However, the current environmental risk assessment framework of chemicals mainly evaluates the parent compounds based on the physicochemical properties and toxicity data and rarely considers their transformation products (TPs), which hinders a comprehensive assessment of the environmental impacts of chemicals.[28] The development of an environmental risk assessment covering potential toxic TPs for linalool is of great significance. The atmospheric transformation mechanism of linalool is currently unclear, especially for hydroxy linalool peroxy radicals (RO_2·) formed by continuous ·OH and O_2 addition.[28,30−32] Subsequent transformations of hydroxy linalool RO_2· were assumed to react primarily via bimolecular pathways (mainly with NO) to produce various carbonyl compounds. The latest experimental study of ·OH-initiated oxidation of linalool showed a carbon balance of only 22%,[29] suggesting that there are still many undetected oxidation products, which hinders our understanding of the atmospheric fate of linalool. Previous studies were mainly conducted under high NO conditions, assuming that unimolecular reactions of RO_2· were too slow to be significant, leading to an incomplete understanding of atmospheric transformation of linalool under different NO conditions.[30,31] Particularly in indoor air, where the concentration of NO is significantly lower than outdoors, unimolecular reactions of RO_2· become particularly important. Moreover, RO_2· has been associated with the formation of highly oxygenated low-volatile products via autoxidation.[32−37] Structurally, hydroxy linalool RO_2· contains −OH groups, unsaturated double bonds, and long alkyl carbon chains. The −OH groups and C═C bond could promote RO_2· to undergo a rapid H-shift reaction due to their ability to activate α-H atoms.[37,38] The unsaturated C═C bond also makes the ring closure of linalool RO_2· possible.[39] Even the alkyl carbon chain could trigger autoxidation through conversion between RO_2· and RO·.[40] Considering the complex structure of linalool−RO_2· and the concentration of NO in a linalool emission environment,[24] accurately predicting the atmospheric oxidation mechanism of linalool is a critical step in fully assessing the environmental risks of linalool.

In this work, we investigated the atmospheric chemistry of linalool using a combination of quantum chemical calculations and kinetics modeling. Four hydroxy linalool RO_2· (see Figure S1 in the Supporting Information (SI)) derived from ·OH-initiated oxidation of linalool were selected as model compounds. The reaction of selected RO_2· and further transformation of the resulting main intermediates were considered in both indoor and polluted urban environments. Furthermore, the potential environmental toxicity and health effects of their TPs were also assessed by computational toxicology simulations. By investigating the transformation mechanism of hydroxy linalool RO_2· under different NO conditions, we aim to elucidate the fundamental chemistry of linalool. This research will also provide insights for the safe development and application of linalool, including a risk assessment covering its TPs.

2. COMPUTATIONAL METHODS

2.1. Electronic Structure and Energy Calculations

The electronic structure and energy calculations in this study were performed by using the Gaussian 16 program. Geometric optimization and vibrational frequency calculations of reactants, intermediates (IM), transition states (TS), and products (P) were performed at the M06-2X/6-31+G(d,p) level of theory. The connection of each TS between designated local minima can be confirmed by intrinsic reaction coordinate calculations. The zero-point energy correction was obtained at the M06-2X/6-31+G(d,p) theoretical level, and the single-point energy calculation was performed at the M06-2X/6-311+G(3df,2p) theoretical level. The combination of M06-2X/6-31+G(d,p) and M06-2X/6-311+G(3df,2p) has previously been used to study the transformation of RO_2·.[41−43] The accuracy of the selected method has been demonstrated by our recent benchmark study to be comparable to the gold calculation method of ROHF-ROCCSD(T)-F12a/cc-pVDZ-F12.[42]

Considering the effect of multiconformers of reactants and TS on the transformation mechanism, we adopted a combination of single-conformer and multiconformer approximations to study the transformation mechanism by balancing accuracy and computational cost. Based on the calculation results by a single conformer, only the effect of multiconformers is considered for the key reaction pathway of hydroxy linalool RO_2·. Similar to our previous study,[42] a funneling scheme (Scheme S1) by using the Molclus[44] and Gaussian program was employed to search for multiconformers of target reactants and TSs.

2.2. Kinetics Calculations

The reaction rate coefficients of the unimolecular reactions were calculated by using the unimolecular rate theory coupled with the energy-grained master equation for collisional energy transfer (RRKM-ME). The RRKM-ME calculations were carried out using the MESMER package based on the sum and density of rovibrational states from the M06-2X/6-31+G(d,p) structures and M06-2X/6-311+G(3df,2p) energy barrier heights.[45] A single exponential down model was used to approximate the collisional energy transfer with an $\langle \Delta E \rangle_{down}$ of 200 cm^{-1}. The Lennard-Jones parameters of intermediates were estimated using the method of Gilbert and Smith[46] and have been listed in Table S1. The asymmetric Eckart model was used for the tunneling correction factors of H-shift reactions.[47] For selected key reaction pathways, reaction factors were employed to account for the effect of multiconformers on reaction kinetics. The reaction factor is calculated by $k_{SC\text{-}TST}/k_{MC\text{-}TST}$, where $k_{SC\text{-}TST}$ and $k_{MC\text{-}TST}$ are the single-conformer and multiconformer reaction rate coefficients, respectively. The details of the calculation formula are presented in the SI, and the Boltzmann distributions and corresponding $k_{SC\text{-}TST,i}$ and $k_{MC\text{-}TST}$ of reactant conformers in the critical reaction pathways are listed in Table S2 and Table S3.

2.3. Toxicity Assessment

Identified TPs of linalool with the corresponding mass yields or concentrations were used to assess their toxic evolution. The toxicity prediction was achieved using the toxicity estimation software tool (TEST)[48] and ADMETlab 2.0[49] based on the methods of the group contribution method, nearest neighbor method, and quantitative structure−activity relationship model. The oral rat was selected as the test organism for terrestrial toxicity, and the oral rat LD50 was calculated by TEST software. ADMETlab 2.0 software was used to predict the health effects of linalool and its TPs on absorption, distribution, metabolism, excretion, and toxicity (ADMET) related parameters in six toxicity end points, including: AMES toxicity, carcinogenicity, skin sensitization, eye corrosion, and respiratory toxicity. The usefulness and reliability of TEST and ADMETlab 2.0 software have been previously demonstrated, with excellent overall

https://doi.org/10.1021/envhealth.4c00033
Environ. Health 2024, 2, 486−498

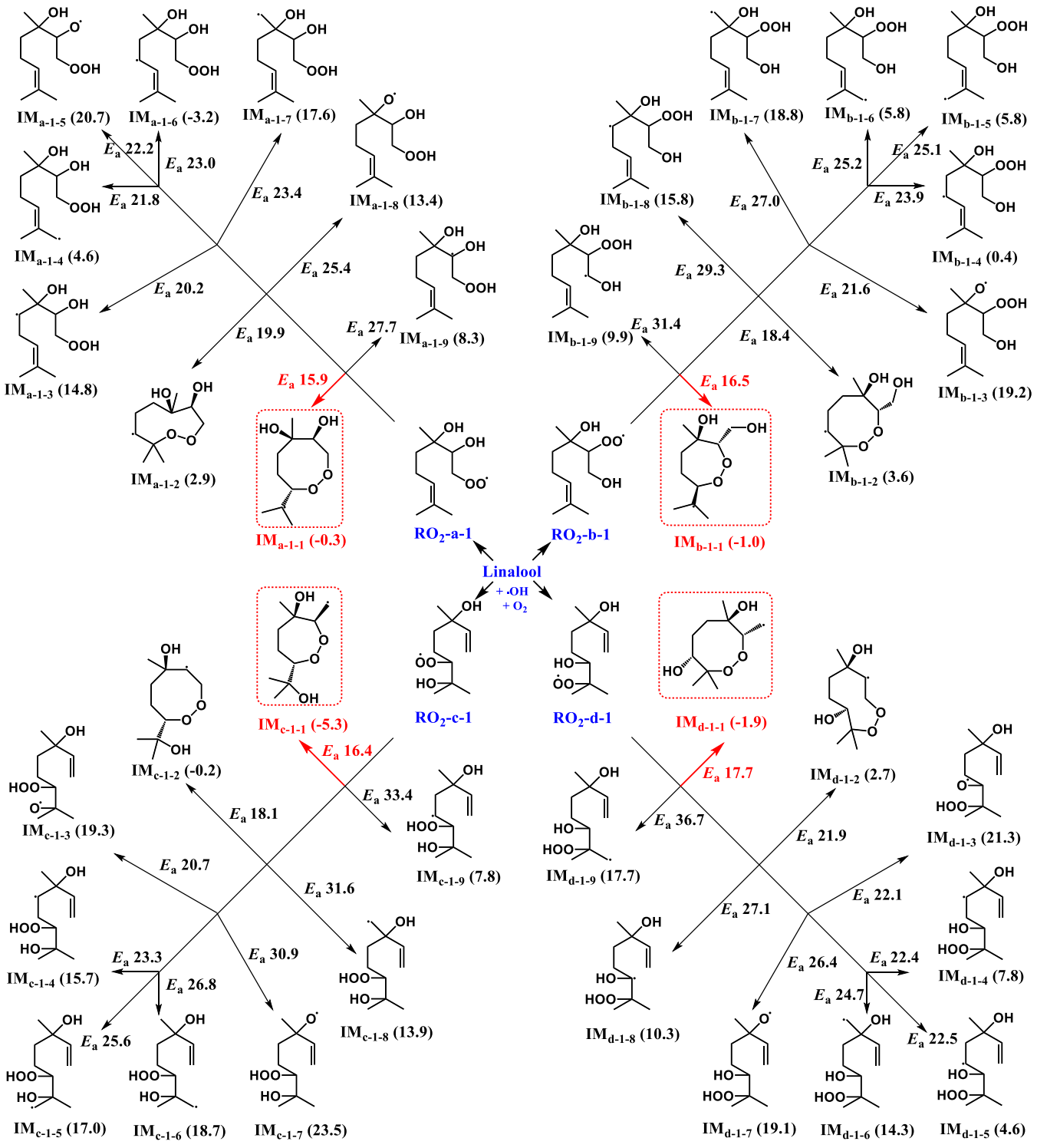

Figure 1. Schematic reaction products with reaction energy (ΔE, in parentheses) and reaction energy barrier (E_a, in kcal mol^{-1}) for unimolecular reactions of hydroxy linalool RO$_2$-*n*-1 (*n* = a, b, c, d) at the M06-2X/6-311+G(3df,2p)//M06-2X/6-31+G(d,p) level of theory.

effect-predictive ability to assess the toxicity of organic pollutants.[49−52]

3. RESULTS AND DISCUSSION

3.1. First Stage of Atmospheric Transformations of Hydroxy Linalool RO$_2$-*n*-1 (*n* = a, b, c, d)

There are mainly two types of reaction pathways in all possible unimolecular reaction pathways of RO$_2$-*n*-1 (*n* = a, b, c, d) (Figure 1). One is the H-shift reaction where the H atom was shifted from the different C atoms to the end site of the −OO group to form R·OOH via 1,*x* H-shift reactions (*x* = 4−9). The other is cyclization reactions via the terminal O atom attacking the C═C bond to form cycloperoxide-R· with *m*-membered (*m* = 7−9) rings. As can be seen from Figure 1 and potential energy surfaces (PES) in Figure S4, reaction energy barriers (E_a) of cyclization pathways are lower than that of H-shift reactions for RO$_2$-*n*-1. The most favorable unimolecular

https://doi.org/10.1021/envhealth.4c00033
Environ. Health 2024, 2, 486−498

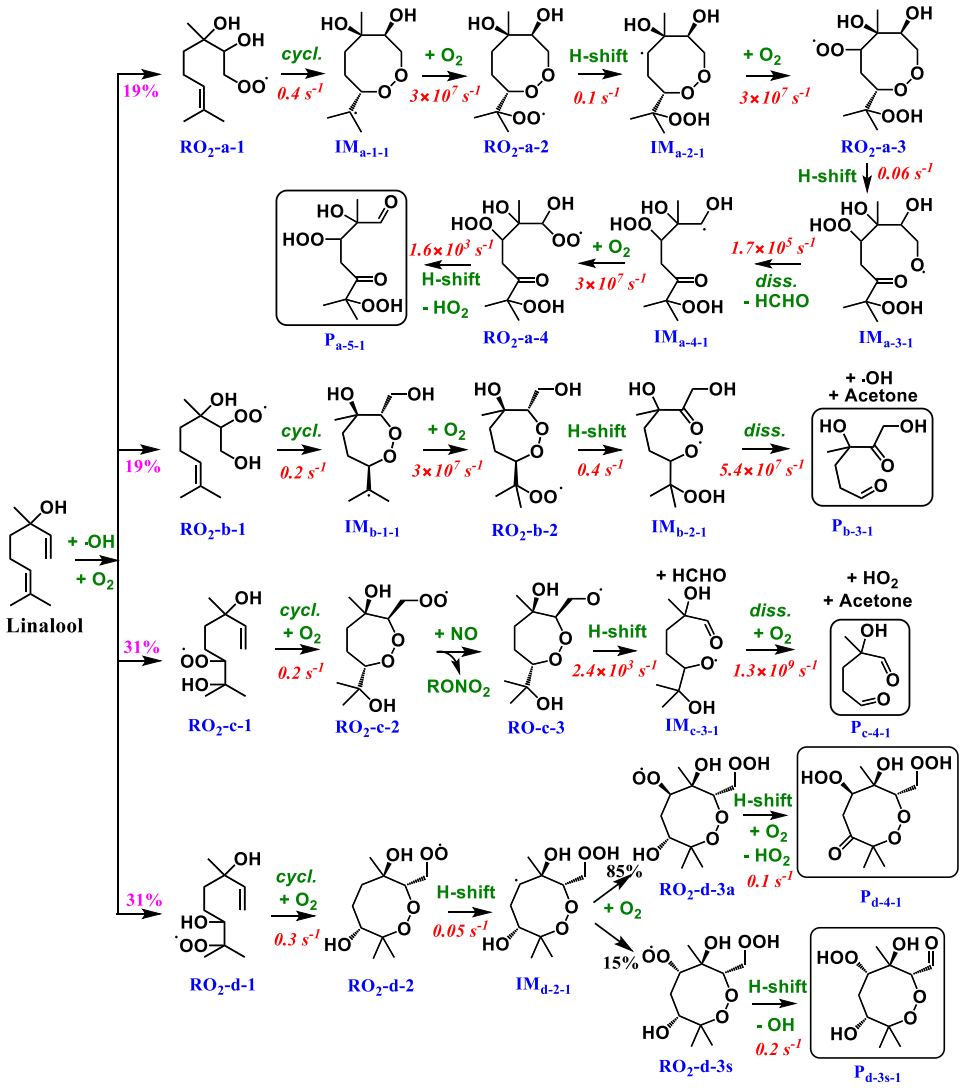

Figure 2. Main atmospheric oxidation mechanisms of linalool-RO_2· under 50 ppt of NO and 1.6 ppt of HO_2· conditions. The MC-TST reaction rate coefficients for the crucial reaction pathways are presented in red italic numbers. The initial fractional yields of RO_2-*n*-1 (*n* = a, b, c, d) are referenced from the experimental results by Bernard et al.[29]

reaction pathways of RO_2-*n*-1 can produce cycloperoxide-R· where the C═C bond being broken lies outside the newly formed 8-membered rings for $IM_{a\text{-}1\text{-}1}$ and $IM_{d\text{-}1\text{-}1}$ or 7-membered rings for $IM_{b\text{-}1\text{-}1}$ and $IM_{c\text{-}1\text{-}1}$. The second competitive reaction pathways of RO_2-*n*-1 are the formation of 9-membered cycloperoxide-R· of $IM_{a\text{-}1\text{-}2}$ and $IM_{d\text{-}1\text{-}2}$ or 8-membered cycloperoxide-R· of $IM_{b\text{-}1\text{-}2}$ and $IM_{c\text{-}1\text{-}2}$, respectively, where the double bond being broken lies inside.

3.1.1. Kinetics. The MESMER software was employed to calculate the reaction rate constants and fractional yields for the favorable reaction pathways (RO_2-*n*-1 → $IM_{n\text{-}1\text{-}1}$ → $IM_{n\text{-}1\text{-}1}$ + O_2 (RO_2-*n*-2); RO_2-*n*-1 → $IM_{n\text{-}1\text{-}2}$ → $IM_{n\text{-}1\text{-}2}$ + O_2 (RO_2-*n*-2′)). Analogous to the well-known transformation of alkyl RO_2·,[53] hydroxy linalool RO_2· can undergo unimolecular reactions or bimolecular reactions with NO, HO_2·, NO_2, and other RO_2·. The corresponding reaction rates of unimolecular or bimolecular reactions determine which of them is dominant. Due to the thermal instability of products resulting from the reaction between RO_2· and NO_2, alongside the low concentrations of other RO_2· species, unimolecular reactions of RO_2· generally encounter competition with bimolecular reactions of NO/HO_2·.[53−55] Thus, bimolecular reactions of RO_2-*n*-1 with NO/HO_2· to form organonitrates and RO· (denoted as P-NO-RO_2-*n*-1) and hydroperoxides and RO· (P-HO_2-RO_2-*n*-1) are considered as possible competitive reactions. Additionally, the bimolecular reaction rate coefficients of RO_2· with NO/HO_2· are largely independent of the structure of RO_2· and are mostly governed by [NO] and [HO_2·]. Under a pristine indoor environment, [NO] is about 50 ppt.[33,34,56−59] Under normal indoor conditions, the highest [HO_2·] is 1.6 ppt.[60] The combined bimolecular RO_2· reactions with NO/HO_2· have pseudo-first-order rate coefficients of 1.2 × 10^{-2} s^{-1} indoors by adopting the typical rate coefficient of k_{RO2+NO} = 9.0 × 10^{-12} molecules cm^{-3} s^{-1}[61] and $k_{RO2+HO2}$ = 1.7 × 10^{-11} molecules cm^{-3} s^{-1}.[61,62] Under an urban atmosphere, [NO] and [HO_2·] are approximately 10 ppb and 5 ppt,[36] respectively, which results in the corresponding pseudo-first-order rate coefficients of bimolecular RO_2· reactions with NO/HO_2· being 2.3 s^{-1}. The relevant simulation details are presented in SI. The calculated time-dependent fractional yields of the main TPs from ·OH-linalool + O_2 reactions are presented in Figure S2 and Figure S3.

https://doi.org/10.1021/envhealth.4c00033
Environ. Health 2024, 2, 486−498

Based on the multiconformer transition state theory (MC-TST), the calculated reaction rate coefficients forming $IM_{a\text{-}1\text{-}1}$, $IM_{b\text{-}1\text{-}1}$, $IM_{c\text{-}1\text{-}1}$, and $IM_{d\text{-}1\text{-}1}$ from RO_2-*n*-1 are 0.4 s^{-1}, 0.2 s^{-1}, 0.2 s^{-1}, and 0.3 s^{-1}, respectively, which are higher than that of the competitive inner ring radicals $IM_{a\text{-}1\text{-}2}$ (2.2×10^{-4} s^{-1}), $IM_{b\text{-}1\text{-}2}$ (6.9×10^{-4} s^{-1}), $IM_{c\text{-}1\text{-}2}$ (4.1×10^{-4} s^{-1}), and $IM_{d\text{-}1\text{-}2}$ (1.9×10^{-5} s^{-1}). Recent studies have suggested that the formation of ring closure products with the radical center lying outside the ring through exocyclization of RO_2· is more favorable than the formation of inner ring radicals by its endocyclization.[63] Even some endocyclization reactions with small ring members are not feasible by Baldwin's rules.[64] Similarly, a structure−activity relationship study has also shown that ring closure of RO_2· on the nearer unsaturated carbon is more favorable because it does not have a rigid olefin structure in the transition state cycle.[39] These previously revealed patterns of ring closure reactions in unsaturated RO_2· can further support our calculation results that the main products of unimolecular reactions for RO_2-*n*-1 are the cycloperoxide-R· of $IM_{n\text{-}1\text{-}1}$ through exocyclization reactions, while the products from endocyclization and H-shift reaction channels are negligible. As shown in Figure S2, the formation of new peroxy radicals RO_2-*n*-2 via successive exocyclization and O_2-addition is the most favorable for RO_2-*n*-1, followed by the formation of P-NO-RO_2-*n*-1 via bimolecular reactions under 50 ppt NO and 1.6 ppt HO_2· conditions. In fact, the propagation of the radical center from RO_2-*n*-1 to RO_2-*n*-2 via the ring closure and O_2-addition reaction essentially follows a new type of autoxidation mechanism, which is different from the widely accepted concept of H-shift-driven autoxidation.[35,36]

Since the formed RO_2-*n*-2 are active intermediates with high fractional yields, their further transformation will be investigated under indoor air conditions with [NO] of 50 ppt and [HO_2] of 1.6 ppt.[33,34,57,60] In addition, considering the outdoor emission of linalool and its transfer from indoor to outdoor conditions, the transformation mechanism of linalool-RO_2· under outdoor atmospheric conditions is also worthy of attention. Under high NO conditions, the bimolecular reactions of RO_2-*n*-1 with NO will dominantly form P-NO-RO_2-*n*-1 (Figure S3), including alkoxy radicals RO-*n*-1, and organonitrates. Therefore, the subsequent transformation of RO-*n*-1 is also discussed in an outdoor atmosphere with typical [NO] and [HO_2·] of 10 ppb and 5 ppt, respectively.[36]

3.2. Further Transformation Mechanisms of RO_2-*n*-2 and Their Main Intermediates in Indoor Air ([NO] = 50 ppt and [HO_2·] = 1.6 ppt)

The calculated schematic PES for all possible unimolecular reactions of RO_2-*n*-2 (*n* = a, b, c, d) and subsequent transformation of key intermediates are presented in Figures S5−S18, and the most favorable reaction pathways are shown in Figure 2. For RO_2-a-2, the most favorable unimolecular reaction pathway is the 1,6-H shift and the addition of O_2 to produce new peroxy radical RO_2-a-3. It noted that the most favorable unimolecular reaction pathway for the unsubstituted 8-membered cycloperoxide-RO_2· is also the 1,6-H shift reaction with the same location of the H atom we found here.[39] In contrast, there are two additional methyl group substituents adjacent to the −OO group and multiple substituents around the 8-membered ring of RO_2-a-2, accelerating this 1,6-H shift reaction. The calculated MC-TST reaction rate constant of forming $IM_{a\text{-}2\text{-}1}$ is 0.1 s^{-1}, which can outrun the corresponding bimolecular reactions of RO_2 indoors (1.2×10^{-2} s^{-1}), indicating that the formation of RO_2-a-3 is feasible in indoor air. RO_2-a-3 can further undergo rapid unimolecular reactions via a 1,5-H shift from the tertiary C6-atom with a high MC-TST reaction rate of 0.06 s^{-1}. Then the ring breaking is spontaneous to form the alkoxy radical $IM_{a\text{-}3\text{-}1}$, which can eventually decompose into formaldehyde, HO_2·, and the closed-shell product $P_{a\text{-}5\text{-}1}$ ($C_9H_{16}O_7$) through rapid C−C bond rupture and recombination with O_2.

As shown in Figure 2, the formation of $IM_{b\text{-}2\text{-}1}$ through 1,7-H shift and a spontaneous ring-opening reaction are the most favorable reaction pathway for RO_2-b-2. The calculated MC-TST reaction rate of forming $IM_{b\text{-}2\text{-}1}$ is 0.4 s^{-1}, which is much higher than that of the 1,7-α-peroxide H shift (1.7×10^{-5} s^{-1}) of unsubstituted 7-membered cycloperoxide-RO_2,[39] due to the presence of multiple substituents in RO_2-b-2 on the respective C atoms where the −OO group and the shifted H atom is located, besides some substituents around the ring. The newly formed alkoxy radical $IM_{b\text{-}2\text{-}1}$ can rapidly undergo successive C−C bond and O−O bond rupture to produce dicarbonyl product $P_{b\text{-}3\text{-}1}$ ($C_7H_{12}O_4$) and acetone, accompanied by the regeneration of the OH radical. Similarly, subsequent transformation of RO_2-d-2 is dominated by a unimolecular reaction in indoor air. The highly oxidized products $P_{d\text{-}3s\text{-}1}$ and $P_{d\text{-}4\text{-}1}$ were produced by H-shift-driven autoxidation, considering the attack of the O_2 in different directions of the ring plane.

In contrast, the MC-TST reaction rate of the most favorable 1,6-H shift for RO_2-c-2 to form $IM_{c\text{-}2\text{-}1}$ (8.5×10^{-4} s^{-1}) is much lower than that of the competitive bimolecular reaction indoors (1.2×10^{-2} s^{-1}). Thus, RO_2-c-2 preferentially undergoes the bimolecular reaction with NO/HO_2· to produce alkoxy radical RO-c-3, in addition to organonitrates and hydroperoxides. The transformation of RO-c-3 is dominated by the successive fragmentation reaction through the C−C bond breaking to remove formaldehyde, spontaneous ring-opening reaction, and acetone removal, followed by the recombination with O_2 to form dicarbonyl products $P_{c\text{-}4\text{-}1}$ ($C_6H_{10}O_3$) and HO_2·.

It deserves mentioning that cyclization-driven autoxidation is central to indoor transformation of hydroxy linalool-RO_2·, and the subsequent active RO· intermediates (such as $IM_{a\text{-}3\text{-}1}$, $IM_{b\text{-}2\text{-}1}$, and RO-c-3) also play a significant role in promoting the transfer of radical centers. Under indoor atmospheric conditions, the oxidation of linalool by ·OH can result in a significant production of acetone, with a fractional yield of 0.41 (Table S4), consistent with previous experiments indicating acetone as the primary oxidation product (yield of 0.34) when linalool reacts with ·OH in the absence of NO. This finding indirectly corroborates the reliability of our computational results. However, earlier experimental studies, limited by experimental equipment, failed to detect highly oxidized, low-volatility products, as suggested in our calculations, achieving only a 22% carbon balance. This suggests the need for future related laboratory research.

3.3. Further Transformation Mechanisms of RO-*n*-1 and Their Main Intermediates under Outdoor Atmospheric Conditions ([NO] = 10 ppb and [HO_2·] = 5 ppt)

The calculated schematic PES of all potential reaction pathways for RO-*n*-1 (*n* = a, b, c, d) and subsequent transformation of dominant intermediates are presented in Figures S19−S30, and the most favorable reaction pathways are also shown in Figure 3. Our calculated MC-TST reaction

https://doi.org/10.1021/envhealth.4c00033
Environ. Health 2024, 2, 486−498

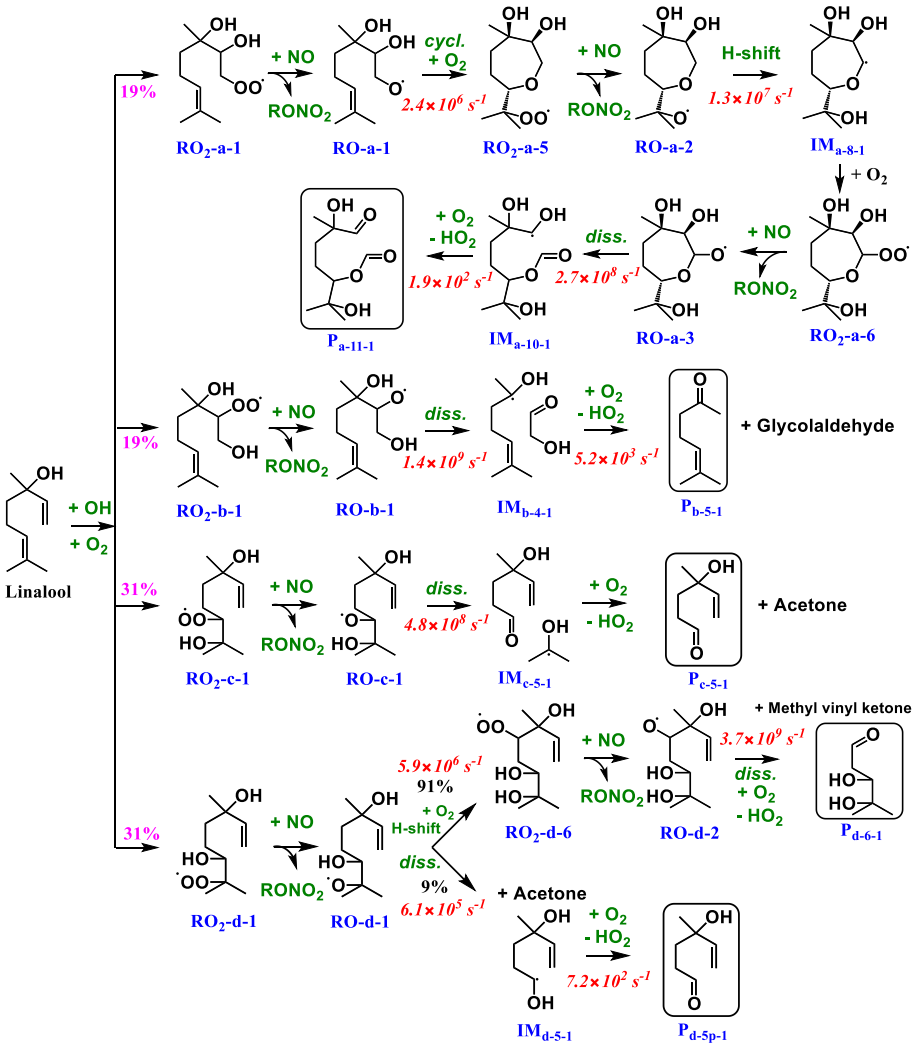

Figure 3. Main atmospheric oxidation mechanisms of linalool-RO_2· under 10 ppb of NO and 5 ppt of HO_2· conditions. The MC-TST reaction rate coefficients for the crucial reaction pathways are presented in red italic numbers. The initial fractional yields of RO_2-*n*-1 (*n* = a, b, c, d) are referenced from the experimental results by Bernard et al.[29]

rate coefficients for the most favorable 7-membered cyclization (2.4×10^6 s^{-1}) of RO-a-1 are much higher than that of C1−C2 bond rupture (1.5×10^4 s^{-1}). Therefore, the most favorable reaction pathway of RO-a-1 is the formation of epoxide ($IM_{a\text{-}2\text{-}1}$), as opposed to the proposed fragmentation channel of forming formaldehyde and 2,6-dimethyl-2-hydroxy-5-hepten-1-one.[29,30] $IM_{a\text{-}2\text{-}1}$ can rapidly react with O_2 to form a new peroxy radical RO_2-a-5, achieving propagation of the radical center. The most favorable unimolecular reaction pathway of RO_2-a-5 is the formation of $IM_{a\text{-}7\text{-}1}$ through a 1,7-H shift reaction with an MC-TST rate of 0.04 s^{-1}, which can be suppressed by the bimolecular reaction of RO_2-a-5 with NO/HO_2 (2.3 s^{-1}) under outdoor atmosphere conditions, leading to the formation of RO-a-2, besides organonitrates and hydroperoxides. The rapid 1,5-H shift reaction of RO-a-2 and the O_2-addition can produce RO_2-a-6, while its fragmentation channel is not competitive. Although RO_2-a-6 has a fast unimolecular reaction rate of 1.0 s^{-1} via a rapid 1,5-H shift reaction, it is still not enough to compete with its bimolecular reaction (2.3 s^{-1}), resulting in the formation of RO-a-3 as the main intermediate. Finally, RO-a-3 can undergo C−C bond rupture and an H-abstraction reaction by O_2 to generate highly oxidized dicarbonyl compound $P_{a\text{-}11\text{-}1}$ ($C_{10}H_{18}O_5$).

In view of Figure 3, the C−C bond rupture to form $IM_{b\text{-}4\text{-}1}$ and $IM_{c\text{-}5\text{-}1}$, including carbonyl compounds and C-centered radicals, is the most favorable reaction for RO-b-1 and RO-c-1, respectively. The results are consistent with earlier experimental studies and predicted that the fragmentation reactions dominate the transformation of linalool alkoxy radicals.[29,30] The calculated MC-TST reaction rate coefficients of C−C bond rupture of RO-b-1 and RO-c-1 are 1.4×10^9 and 4.8×10^8 s^{-1}, respectively, which is much higher than that of *α*-H-abstraction by O_2, with the pseudo-first-order reaction rates being 11.0 s^{-1} and 35.8 s^{-1} for RO-b-1 and RO-c-1, respectively. Thus, RO-b-1 and RO-c-1 will eventually dissociate to form $P_{b\text{-}5\text{-}1}$ (6-methyl-5-hepten-2-one) and glycolaldehyde, as well as $P_{c\text{-}5\text{-}1}$ (4-hydroxy-4-methyl-5-hexen-1-al) and acetone, respectively.

In contrast, the MC-TST reaction rates of forming $IM_{d\text{-}2\text{-}1}$ and $IM_{d\text{-}2\text{-}2}$ are 6.1×10^5 and 5.9×10^6 s^{-1} through dissociation and 1,5-H shift of RO-d-1, respectively. The MESMER model shows that the fate of RO-d-1 mainly generates the new peroxy radical RO_2-d-6 ($IM_{d\text{-}5\text{-}2} + O_2$) with a fractional yield of 91%, while the predicted dominant fragmentation pathway of forming acetone and 4-hydroxy-4-methyl-5-hexen-1-al derived from $IM_{d\text{-}2\text{-}1}$ by early experiments

https://doi.org/10.1021/envhealth.4c00033
Environ. Health 2024, 2, 486−498

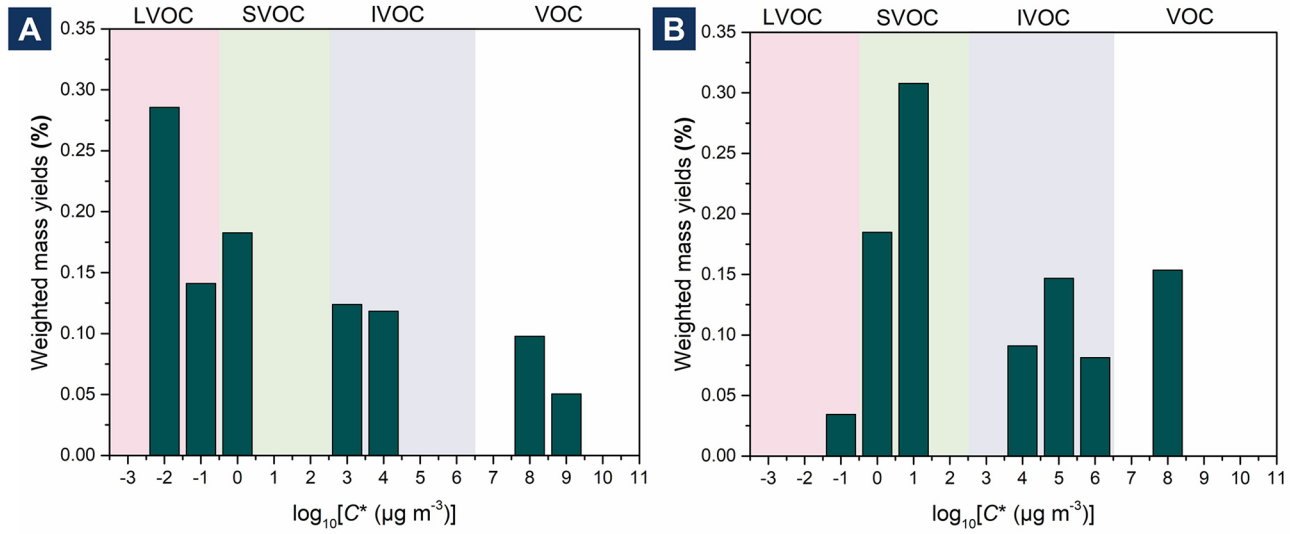

Figure 4. Volatility distribution of transformation products based on a one-dimensional volatility basis set from different reaction mechanisms of hydroxy linalool RO_2· under (A) the indoor air with low NO concentrations and isomerization-dominated and (B) the outdoor environment with high NO concentrations dominated by bimolecular reaction with NO.

only accounts for 9%. Under a polluted outdoor atmosphere, the bimolecular reaction of RO_2-d-6 with NO/HO_2 could inhibit the occurrence of cyclization reaction ($0.07\ s^{-1}$), mainly leading to the formation of RO-d-2. The formed RO-d-2 can eventually generate carbonyl compounds $P_{d\text{-}6-1}$ ($C_6H_{12}O_3$) and methyl vinyl ketone through a fragmentation reaction and H-abstraction involving O_2.

Under high NO conditions, our calculated atmospheric transformation mechanisms of hydroxy linalool RO_2· are consistent with previous experimental results and observed fragmentation products in the oxidation reaction of linalool, further confirming the reliability of our computational findings.[29,30] Our computational results reveal that acetone, $P_{c\text{-}5-1}$, and $P_{b\text{-}5-1}$ are the main products resulting from the reaction of linalool with ·OH outdoors with respective fractional yields of 0.24, 0.24, and 0.14. These results align with earlier experimental findings of acetone (0.50), 4-hydroxy-4-methyl-5-hexen-1-al (0.46), and 6-methyl-5-hept-en-2-one (0.07). Additionally, environmental factors such as humidity, ammonia, and temperature can impact the atmospheric transformation of linalool by altering the reactivity of hydroxy linalool RO_2·. For example, elevated relative humidity can alter the unimolecular reaction capacity of RO_2·;[65] ammonia can facilitate the hydrolysis of carbonyl oxidation products;[66] and high temperatures can enhance the autoxidation of linalool RO_2·.[36] An extensive experimental investigation into product identification during the OH-initiated oxidation of linalool under atmospheric conditions with varying NO concentrations would be highly valuable for fully understanding the influence of environmental factors.

3.4. Volatility Distribution of Transformation Products from Different Reaction Mechanisms of Hydroxy Linalool RO_2· under Indoor or Outdoor Conditions

Hydroxy linalool RO_2· can follow the concerted RO_2· and RO· modulated autoxidation mechanism to produce a large amount of highly oxygenated products with less volatility than that of linalool. In terms of volatility distribution of TPs at different [NO] levels from one-dimensional VBS (Figure 4),[67] the mass yield (0.85) of TPs that are less volatile than linalool indoors was higher than that of TPs (0.62) outdoors; the mass yield of LVOCs (0.43 vs 0.034) was especially much higher indoors than outdoors. More importantly, TPs under low NO conditions are mainly highly oxidized cycloperoxide and dicarbonyl products via cyclization-driven autoxidation that are expected to significantly contribute to SOA formation via reactive uptake,[68−71] while organonitrates are the main product to contribute to the formation of SOA by gas-particle partitioning under high NO conditions. The detailed molecular mechanisms of the concerted RO_2· and RO· modulated autoxidation and volatility distribution of TPs in this study open avenues for explaining the high SOA yield from ·OH-initiated oxidation of linalool,[29] especially under low NO conditions with RO_2· and RO· being isomerization-dominated.

3.5. Toxicity Assessment during Atmospheric Transformation of Linalool

We evaluated the toxicity evolution of linalool and TPs to terrestrial test organism rats and humans. During the atmospheric transformation of linalool, more than half of TPs (Figure 5A), especially for $P_{d\text{-}4-1}$, $P_{a\text{-}5-1}$, formaldehyde, glycolaldehyde, methyl vinyl ketone (MVK), and all organonitrates ($RONO_2$), exhibited higher toxicities to rats than the parent compound linalool, classifying as "low toxic", "moderately toxic", or even "very toxic". Linalool, as a VCP originally considered safe, is mainly used in indoor environments, where the fractional mass yields of TPs that are more toxic than linalool are higher than that of outdoor atmospheric conditions. Further assessment of the carcinogenicity and respiratory toxic effects of TPs is presented in Figure 5B and 5C, and a similar probability of mutagenicity, skin sensitization, and eye irritation are also presented in Figure S31. There are also many TPs with a toxic effect higher than that of linalool. More interestingly, highly oxygenated low-volatility TPs that are more easily formed indoors have higher carcinogenicity and respiratory toxicity than outdoor TPs. Thus, the potential risks of linalool in indoor environments are of concern, and it is especially recommended to pay attention to the environmental impacts of indoor TPs.

https://doi.org/10.1021/envhealth.4c00033
Environ. Health 2024, 2, 486−498

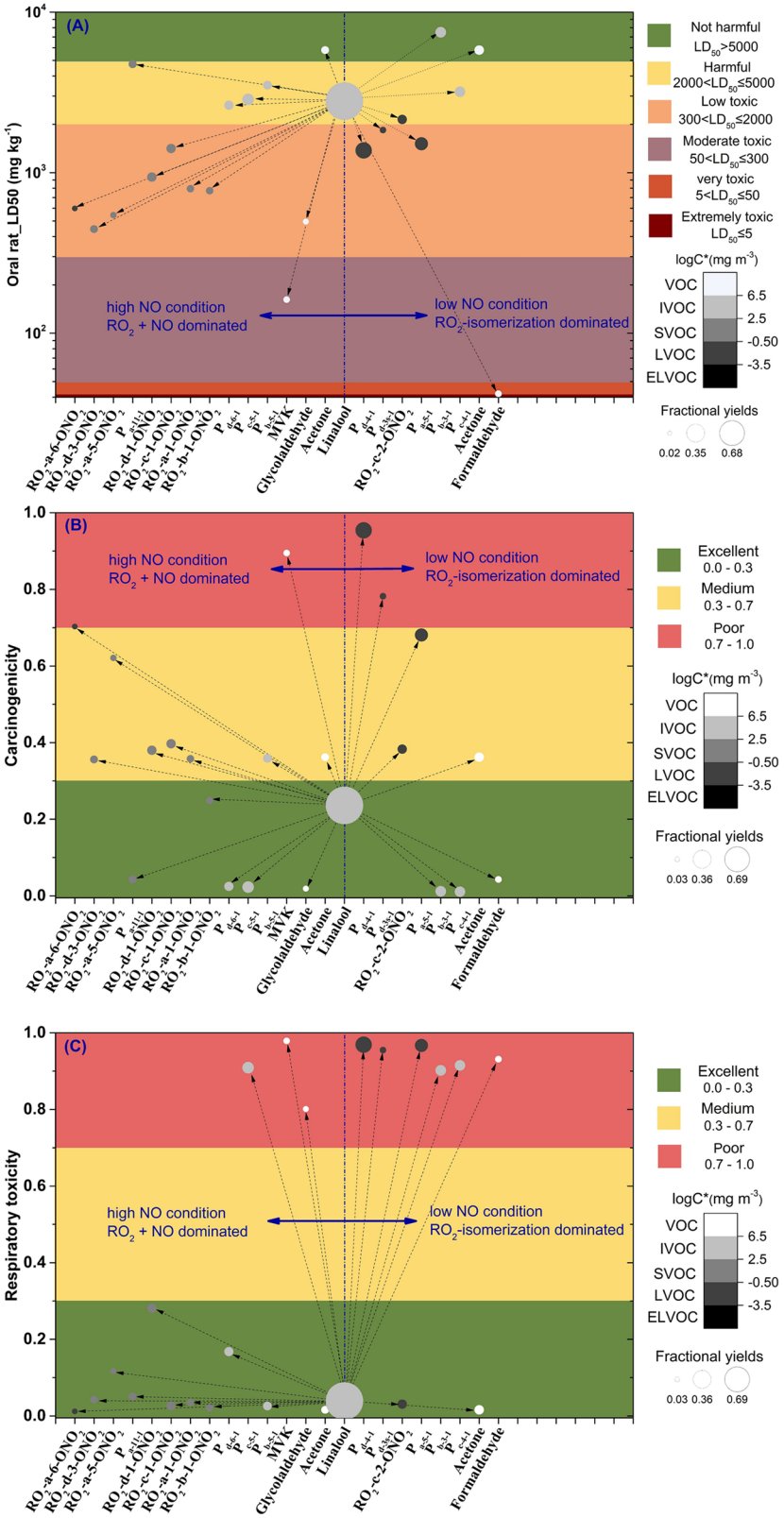

Figure 5. Predicted value of (A) rat oral acute toxicity, (B) carcinogenicity, and (C) respiratory toxic effects of linalool and its main atmospheric transformation products under different NO levels. The output values of carcinogenicity and respiratory toxic effects are the probability of being toxic, within the range of 0 to 1. Volatility distribution and fractional mass yields of transformation products of linalool are also shown in the diagram.

In fact, by considering that TPs with strong toxicity indicators may not lead to high toxicity due to the limited atmospheric lifetime, this extrapolation cannot be made without considering the further atmospheric transformation of TPs. Since the reaction rate of hydroxy linalool RO_2· is much higher than the corresponding ·OH-initiated reaction of

https://doi.org/10.1021/envhealth.4c00033
Environ. Health 2024, 2, 486−498

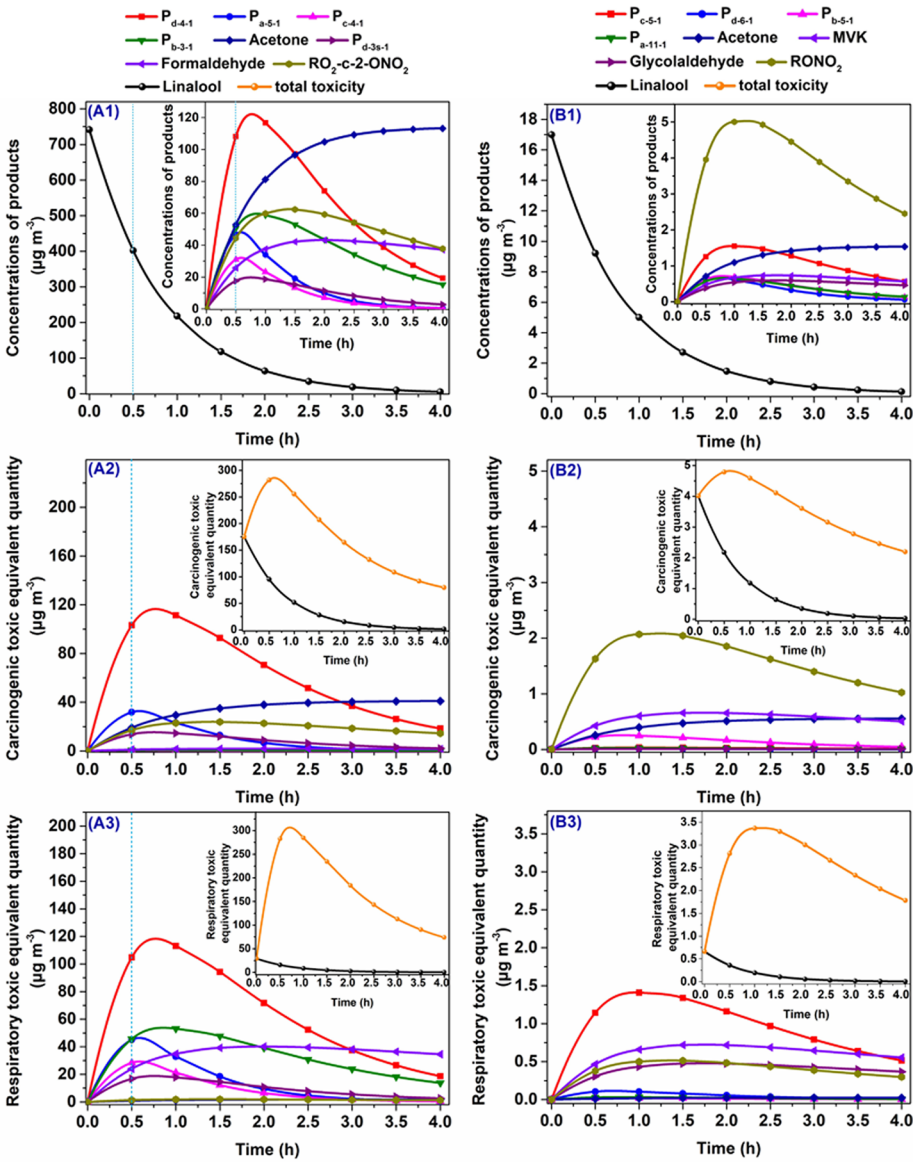

Figure 6. Atmospheric concentrations and carcinogenic and respiratory toxic equivalent quantities of transformation products from linalool, considering their subsequent transformation under indoor (A1, A2, A3) and outdoor (B1, B2, B3) atmosphere conditions, respectively. It is noted that "$RONO_2$" represents the total set of RO_2-*n*-1-$RONO_2$ (*n* = a, b, c, d), RO_2-d-3-$RONO_2$, RO_2-a-5-$RONO_2$, and RO_2-a-6-$RONO_2$.

linalool, the formation concentrations of TPs over time with considering their further atmospheric transformation can be calculated as

$$[TPi] = [\mathrm{R}] \times (1 - \exp(-k\_\mathrm{R} \times [\cdot\mathrm{OH}] \times t) \times \Gamma\_TPi \times \exp(-k\_TPi \times [\cdot\mathrm{OH}] \times t))$$

and the total toxicity of linalool and TPs can be computed as follows: $\Sigma\mathrm{TEQ}i = \mathrm{TEF}i \times Ci$, where $[TPi]$, [R], and [·OH] represent concentrations of different TPs, linalool, and ·OH, respectively; k_R and k_TPi are the reaction rate constants of ·OH with linalool (1.7×10^{-10} cm^3 $molecule^{-1}$ s^{-1}) and different TPs (see Table S4 for details); Γ_TPi are the fractional yields of *TPi* in the autoxidation reaction of linalool (Table S4); *t* is the reaction period (4 h corresponding to indoor cleaning and the same time outdoors for comparison); TEQ is the toxic equivalent quantity; TEF is the toxic equivalency factor, such as carcinogenic and toxic respiratory effects; and *Ci* represents mass concentrations of linalool and TPs. The average concentration of linalool was 741.5 $\mu g\ m^3$ in the indoor air when using the indoor-cleaning products and 17.0 $\mu g\ m^3$ in the outdoor air, respectively.[24,25,27] During indoor cleaning, indoor [·OH] could be comparable to outdoor conditions up to 2×10^6 molecules cm^{-3}.[72] Based on the above, the concentrations, carcinogenics, and respiratory toxic equivalent quantity of the key TPs from linalool and their subsequent transformation under indoor and outdoor air conditions are shown in Figure 6. Under indoor air conditions, $P_{d\text{-}4\text{-}1}$, RO_2-c-2-ONO_2, and $P_{b\text{-}3\text{-}1}$ have high atmospheric concentrations and long atmospheric lifetimes (Figure 6A1). Considering their respective toxic effects, $P_{d\text{-}4\text{-}1}$ and RO_2-c-2-ONO_2 show high carcinogenicity (Figure 6A2), while $P_{d\text{-}4\text{-}1}$ and $P_{b\text{-}3\text{-}1}$ show high respiratory toxic effects (Figure 6A3). It is noted that if air exchange is considered during indoor cleaning a typical residence time for indoor air could be <0.5 h. TPs of linalool at the initial stage of the reaction (see data points <0.5 h in Figure 6A with the blue dashed line) will drive the toxicity impacts. Furthermore, the

https://doi.org/10.1021/envhealth.4c00033
Environ. Health 2024, 2, 486−498

normal OH concentration indoors is about ~10^5 molecules cm^{-3},[60,73] suggesting the slower consumption rates of indoor linalool-TPs and higher health risk. Similarly, the total organonitrates and $P_{c\text{-}5-1}$ have higher concentrations and longer atmospheric lifetimes than other TPs under outdoor conditions, with particular attention given to the carcinogenicity of organonitrates and respiratory toxicity of $P_{c\text{-}5-1}$. Considering the stronger toxic equivalent quantity of TPs indoors than outdoors, the results of the linalool case further emphasized the urgent need to pay attention to the transformation mechanisms of chemicals in the indoor air and environmental risks of TPs.

4. CONCLUSIONS AND ENVIRONMENTAL IMPLICATION

This study reveals that the concerted RO_2· and RO· modulated autoxidation is a key mechanistic step for the atmospheric transformation of linalool, highlighting the importance of cyclization reactions of both RO_2· and RO· in the indoor and polluted outdoor air, representing the low and high NO/HO_2· levels, respectively. To the best of our knowledge, this is one of the few cases in which functionalized reactive organic intermediates have been shown to undergo successive transformation of the radical center in multiple ways, including RO_2·-dominated cyclization and H-shift combined with RO·-dominated cyclization, H-shift, and bond scission, to follow the novel autoxidation mechanism. The traditional RO_2·-dominated autoxidation generally occurs in the atmospheric oxidation of VOCs containing multiple reactive functional groups, while the generalized RO_2· and RO·-driven autoxidation mechanisms would be more important for atmospheric transformation of unsubstituted aromatics, olefins, and even long-chain alkanes. The feasibility of the generalized autoxidation should pay attention to the radical production and sinks in which they generate functionalized products, especially for the isomerization of active RO· and its competition with a fragmentation reaction in the future. In addition, our study found that linalool has different oxidation mechanisms and products under low and high NO conditions corresponding to indoor and outdoor environments. The key pathways and reaction rates are summarized in Table S5 and Table S6, laying the groundwork for developing chemical transport models for linalool, with a specific focus on the influence of NO on its oxidation mechanism, TPs, ozone forming potential (section S8 in Supporting Information), and SOA yield.

This study established a time-dependent risk assessment method combining the reaction mechanism of linalool and the atmospheric lifetime of TPs. This method also considers different NO concentrations, so it can assess the long-term indoor and outdoor toxic impacts, which could be further improved in the future to obtain a dynamic risk assessment. Our analysis emphasized that high indoor concentrations and a strong emission source coupled with slow consumption rates can lead to significant health risks, particularly when individuals spend extended periods indoors. It is recommended that similar analyses be conducted for other potentially harmful VCPs or specific sources in order to evaluate their emissions and transformation processes on human health. The atmospheric transformation of linalool obviously impacts the current understanding of air chemistry and health effects. Certainly, more efforts to develop environmental risk assessment of chemicals covering their TPs in the future are of great significance to comprehensively assess the environmental risks of VCPs.

■ ASSOCIATED CONTENT

Supporting Information

The Supporting Information is available free of charge at https://pubs.acs.org/doi/10.1021/envhealth.4c00033.

Details of global minima structures of hydroxy linalool RO_2·; flowchart for the multiconformers search; the Lennard-Jones parameters of intermediates; the effect of multiconformers on reaction kinetics; the time-dependent fractional yields of the main transformation products from linalool; calculated schematic potential energy surfaces; toxicity assessment of products formed in atmospheric transformation of linalool (PDF)

Cartesian coordinates (XLSX)

■ AUTHOR INFORMATION

Corresponding Authors

Song Guo − *State Key Joint Laboratory of Environmental Simulation and Pollution Control, International Joint Laboratory for Regional Pollution Control, Ministry of Education (IJRC), College of Environmental Sciences and Engineering, Peking University, Beijing 100871, China; Collaborative Innovation Center of Atmospheric Environment and Equipment Technology, Nanjing University of Information Science & Technology, Nanjing 210044, China;* orcid.org/0000-0002-9661-2313; Email: songguo@pku.edu.cn

Hong-Bin Xie − *Key Laboratory of Industrial Ecology and Environmental Engineering (Ministry of Education), School of Environmental Science and Technology, Dalian University of Technology, Dalian 116024, China;* orcid.org/0000-0002-9119-9785; Email: hbxie@dlut.edu.cn

Authors

Zihao Fu − *State Key Joint Laboratory of Environmental Simulation and Pollution Control, International Joint Laboratory for Regional Pollution Control, Ministry of Education (IJRC), College of Environmental Sciences and Engineering, Peking University, Beijing 100871, China*

Ying Yu − *State Key Joint Laboratory of Environmental Simulation and Pollution Control, International Joint Laboratory for Regional Pollution Control, Ministry of Education (IJRC), College of Environmental Sciences and Engineering, Peking University, Beijing 100871, China*

Shiyu Li − *State Key Joint Laboratory of Environmental Simulation and Pollution Control, International Joint Laboratory for Regional Pollution Control, Ministry of Education (IJRC), College of Environmental Sciences and Engineering, Peking University, Beijing 100871, China*

Daqi Lv − *State Key Joint Laboratory of Environmental Simulation and Pollution Control, International Joint Laboratory for Regional Pollution Control, Ministry of Education (IJRC), College of Environmental Sciences and Engineering, Peking University, Beijing 100871, China*

Putian Zhou − *Institute for Atmospheric and Earth System Research/Physics, Faculty of Science, University of Helsinki, FIN-00014 Helsinki, Finland*

Kai Song − *State Key Joint Laboratory of Environmental Simulation and Pollution Control, International Joint Laboratory for Regional Pollution Control, Ministry of*

Education (IJRC), College of Environmental Sciences and Engineering, Peking University, Beijing 100871, China

Zheng Chen − *State Key Joint Laboratory of Environmental Simulation and Pollution Control, International Joint Laboratory for Regional Pollution Control, Ministry of Education (IJRC), College of Environmental Sciences and Engineering, Peking University, Beijing 100871, China*

Rui Tan − *State Key Joint Laboratory of Environmental Simulation and Pollution Control, International Joint Laboratory for Regional Pollution Control, Ministry of Education (IJRC), College of Environmental Sciences and Engineering, Peking University, Beijing 100871, China*

Kun Hu − *State Key Joint Laboratory of Environmental Simulation and Pollution Control, International Joint Laboratory for Regional Pollution Control, Ministry of Education (IJRC), College of Environmental Sciences and Engineering, Peking University, Beijing 100871, China*

Ruizhe Shen − *State Key Joint Laboratory of Environmental Simulation and Pollution Control, International Joint Laboratory for Regional Pollution Control, Ministry of Education (IJRC), College of Environmental Sciences and Engineering, Peking University, Beijing 100871, China*

Maosheng Yao − *State Key Joint Laboratory of Environmental Simulation and Pollution Control, International Joint Laboratory for Regional Pollution Control, Ministry of Education (IJRC), College of Environmental Sciences and Engineering, Peking University, Beijing 100871, China;* orcid.org/0000-0002-1442-8054

Min Hu − *State Key Joint Laboratory of Environmental Simulation and Pollution Control, International Joint Laboratory for Regional Pollution Control, Ministry of Education (IJRC), College of Environmental Sciences and Engineering, Peking University, Beijing 100871, China*

Complete contact information is available at: https://pubs.acs.org/10.1021/envhealth.4c00033

Notes

The authors declare no competing financial interest.

■ ACKNOWLEDGMENTS

This study was supported by the National Natural Science Foundation of China-Creative Research Group Fund (22221004), National Natural Science Foundation of China (22306002), the National Key Research and Development Program of China (2022YFC3701000, Task 2), the China Postdoctoral Science Foundation (2023M730054), the ACCC Flagship funded by the Academy of Finland (337549), and the European Commission Horizon Europe project FOCI (101056783). We thank the Supercomputing Center of Peking University for computational resources.

■ REFERENCES

(1) Vermeulen, R.; Schymanski, E. L.; Barabási, A.-L.; Miller, G. W. The exposome and health: Where chemistry meets biology. *Science* **2020**, *367*, 392−396.

(2) Escher, B. I.; Stapleton, H. M.; Schymanski, E. L. Tracking complex mixtures of chemicals in our changing environment. *Science* **2020**, *367*, 388−392.

(3) Guo, S.; Hu, M.; Peng, J.; Wu, Z.; Zamora, M. L.; Shang, D.; Du, Z.; Zheng, J.; Fang, X.; Tang, R.; Wu, Y.; Zeng, L.; Shuai, S.; Zhang, W.; Wang, Y.; Ji, Y.; Li, Y.; Zhang, A. L.; Wang, W.; Zhang, F.; Zhao, J.; Gong, X.; Wang, C.; Molina, M. J.; Zhang, R. Remarkable nucleation and growth of ultrafine particles from vehicular exhaust. *Proc. Natl. Acad. Sci. U. S. A.* **2020**, *117* (7), 3427−3432.

(4) Yadav, D.; Rangabhashiyam, S.; Verma, P.; Singh, P.; Devi, P.; Kumar, P.; Hussain, C. M.; Gaurav, G. K.; Kumar, K. S. Environmental and health impacts of contaminants of emerging concerns: Recent treatment challenges and approaches. *Chemosphere* **2021**, *272*, 129492.

(5) Cooper, A. W.; Rogers, M. M.; Wiggin, K. J.; Slade, J. H. We need a "keeling curve" approach for contaminants of emerging concern. *Environ. Sci. Technol.* **2023**, *57* (28), 10147−10150.

(6) McDonald, B. C.; de Gouw, J. A.; Gilman, J. B.; Jathar, S. H.; Akherati, A.; Cappa, C. D.; Jimenez, J. L.; Lee-Taylor, J.; Hayes, P. L.; McKeen, S. A.; Cui, Y. Y.; Kim, S.-W.; Gentner, D. R.; Isaacman-VanWertz, G.; Goldstein, A. H.; Harley, R. A.; Frost, G. J.; Roberts, J. M.; Ryerson, T. B.; Trainer, M. Volatile chemical products emerging as largest petrochemical source of urban organic emissions. *Science* **2018**, *359* (21), 760−764.

(7) Seltzer, K. M.; Pennington, E.; Rao, V.; Murphy, B. N.; Strum, M.; Isaacs, K. K.; Pye, H. O. T. Reactive organic carbon emissions from volatile chemical products. *Atmos. Chem. Phys.* **2021**, *21* (6), 5079−5100.

(8) Gkatzelis, G. I.; Coggon, M. M.; McDonald, B. C.; Peischl, J.; Aikin, K. C.; Gilman, J. B.; Trainer, M.; Warneke, C. Identifying volatile chemical product tracer compounds in u. S. Cities. *Environ. Sci. Technol.* **2021**, *55* (1), 188−199.

(9) Coggon, M. M.; Gkatzelis, G. I.; McDonald, B. C.; Gilman, J. B.; Schwantes, R. H.; Abuhassan, N.; Aikin, K. C.; Arend, M. F.; Berkoff, T. A.; Brown, S. S.; Campos, T. L.; Dickerson, R. R.; Gronoff, G.; Hurley, J. F.; Isaacman-VanWertz, G.; Koss, A. R.; Li, M.; McKeen, S. A.; Moshary, F.; Peischl, J.; Pospisilova, V.; Ren, X.; Wilson, A.; Wu, Y.; Trainer, M.; Warneke, C. Volatile chemical product emissions enhance ozone and modulate urban chemistry. *Proc. Natl. Acad. Sci. U. S. A.* **2021**, *118* (32), e2026653118.

(10) Zhu, W.; Guo, S.; Zhang, Z.; Wang, H.; Yu, Y.; Chen, Z.; Shen, R.; Tan, R.; Song, K.; Liu, K.; Tang, R.; Liu, Y.; Lou, S.; Li, Y.; Zhang, W.; Zhang, Z.; Shuai, S.; Xu, H.; Li, S.; Chen, Y.; Hu, M.; Canonaco, F.; Prévôt, A. S. H. Mass spectral characterization of secondary organic aerosol from urban cooking and vehicular sources. *Atmos. Chem. Phys.* **2021**, *21* (19), 15065−15079.

(11) Chang, X.; Zhao, B.; Zheng, H.; Wang, S.; Cai, S.; Guo, F.; Gui, P.; Huang, G.; Wu, D.; Han, L.; Xing, J.; Man, H.; Hu, R.; Liang, C.; Xu, Q.; Qiu, X.; Ding, D.; Liu, K.; Han, R.; Robinson, A. L.; Donahue, N. M. Full-volatility emission framework corrects missing and underestimated secondary organic aerosol sources. *One Earth* **2022**, *5* (4), 403−412.

(12) Seltzer, K. M.; Murphy, B. N.; Pennington, E. A.; Allen, C.; Talgo, K.; Pye, H. O. T. Volatile chemical product enhancements to criteria pollutants in the united states. *Environ. Sci. Technol.* **2022**, *56* (11), 6905−6913.

(13) Huang, L.; Zhao, B.; Wang, S.; Chang, X.; Klimont, Z.; Huang, G.; Zheng, H.; Hao, J. Global anthropogenic emissions of full-volatility organic compounds. *Environ. Sci. Technol.* **2023**, *57*, 16435.

(14) Pennington, E. A.; Seltzer, K. M.; Murphy, B. N.; Qin, M.; Seinfeld, J. H.; Pye, H. O. T. Modeling secondary organic aerosol formation from volatile chemical products. *Atmos. Chem. Phys.* **2021**, *21* (24), 18247−18261.

(15) Yu, Y.; Guo, S.; Wang, H.; Shen, R.; Zhu, W.; Tan, R.; Song, K.; Zhang, Z.; Li, S.; Chen, Y.; Hu, M. Importance of semivolatile/intermediate-volatility organic compounds to secondary organic aerosol formation from chinese domestic cooking emissions. *Environ. Sci. Technol. Lett.* **2022**, *9* (6), 507−512.

(16) Song, K.; Guo, S.; Gong, Y.; Lv, D.; Zhang, Y.; Wan, Z.; Li, T.; Zhu, W.; Wang, H.; Yu, Y.; Tan, R.; Shen, R.; Lu, S.; Li, S.; Chen, Y.; Hu, M. Impact of cooking style and oil on semi-volatile and intermediate volatility organic compound emissions from chinese domestic cooking. *Atmos. Chem. Phys.* **2022**, *22* (15), 9827−9841.

(17) Sasidharan, S.; He, Y.; Akherati, A.; Li, Q.; Li, W.; Cocker, D.; McDonald, B. C.; Coggon, M. M.; Seltzer, K. M.; Pye, H. O. T.; Pierce, J. R.; Jathar, S. H. Secondary organic aerosol formation from

volatile chemical product emissions: Model parameters and contributions to anthropogenic aerosol. *Environ. Sci. Technol.* **2023**, *57* (32), 11891−11902.
(18) Kamatou, G. P. P.; Viljoen, A. M. Linalool-a review of a biologically active compound of commercial importance. *Nat. Prod. Commun.* **2008**, *3* (7), 1183−1192.
(19) Steinemann, A. C.; MacGregor, I. C.; Gordon, S. M.; Gallagher, L. G.; Davis, A. L.; Ribeiro, D. S.; Wallace, L. A. Fragranced consumer products: Chemicals emitted, ingredients unlisted. *Environ. Impact Assess. Review* **2011**, *31* (3), 328−333.
(20) Bråred Christensson, J.; Karlberg, A.-T.; Andersen, K. E.; Bruze, M.; Johansen, J. D.; Garcia-Bravo, B.; Giménez Arnau, A.; Goh, C.-L.; Nixon, R.; White, I. R. Oxidized limonene and oxidized linalool - concomitant contact allergy to common fragrance terpenes. *Contact Dermatitis* **2016**, *74* (5), 273−280.
(21) Steinemann, A. Volatile emissions from common consumer products. *Air Qual. Atmos. Hlth.* **2015**, *8* (3), 273−281.
(22) Nematollahi, N.; Kolev, S. D.; Steinemann, A. Volatile chemical emissions from 134 common consumer products. *Air Qual. Atmos. Hlth.* **2019**, *12* (11), 1259−1265.
(23) Linalool market: Global industry forecast (2023−2029). https://www.maximizemarketresearch.com/market-report/global-linalool-market/78118/ (accessed November 21, 2023).
(24) Wolkoff, P.; Nielsen, G. D. Effects by inhalation of abundant fragrances in indoor air - an overview. *Environ. Int.* **2017**, *101*, 96−107.
(25) Arey, J.; Corchnoy, S. B.; Atkinson, R. Emission of linalool from valencia orange blossoms and its observation in ambient air. *Atmos. Environ.* **1991**, *25* (7), 1377−1381.
(26) Lamas, J. P.; Sanchez-Prado, L.; Garcia-Jares, C.; Llompart, M. Determination of fragrance allergens in indoor air by active sampling followed by ultrasound-assisted solvent extraction and gas chromatography−mass spectrometry. *J. Chromatogr. A* **2010**, *1217* (12), 1882−1890.
(27) Su, H.-J.; Chao, C.-J.; Chang, H.-Y.; Wu, P.-C. The effects of evaporating essential oils on indoor air quality. *Atmos. Environ.* **2007**, *41* (6), 1230−1236.
(28) Liu, Q.; Li, L.; Zhang, X.; Saini, A.; Li, W.; Hung, H.; Hao, C.; Li, K.; Lee, P.; Wentzell, J. J. B.; Huo, C.; Li, S. M.; Harner, T.; Liggio, J. Uncovering global-scale risks from commercial chemicals in air. *Nature* **2021**, *600* (7889), 456−461.
(29) Bernard, F.; Daële, V.; Mellouki, A.; Sidebottom, H. Studies of the gas phase reactions of linalool, 6-methyl-5-hepten-2-ol and 3-methyl-1-penten-3-ol with o3 and oh radicals. *J. Phys. Chem. A* **2012**, *116* (24), 6113−6126.
(30) Shu, Y.; Kwok, E. S. C.; Tuazon, E. C.; Atkinson, R.; Arey, J. Products of the gas-phase reactions of linalool with oh radicals, no_3 radicals, and o_3. *Environ. Sci. Technol.* **1997**, *31*, 896−904.
(31) Atkinson, R.; Arey, J.; Aschmann, S. M.; Corchnoy, S. B.; Shu, Y. Rate constants for the gas-phase reactions ofcis-3-hexen-1-ol,cis-3-hexenylacetate,trans-2-hexenal, and linalool with oh and no3radicals and o3at 296 ± 2 k, and oh radical formation yields from the o3reactions. *Int. J. Chem. Kinet.* **1995**, *27* (10), 941−955.
(32) Møller, K. H.; Otkjær, R. V.; Chen, J.; Kjaergaard, H. G. Double bonds are key to fast unimolecular reactivity in first-generation monoterpene hydroxy peroxy radicals. *J. Phys. Chem. A* **2020**, *124* (14), 2885−2896.
(33) Chen, J.; Møller, K. H.; Wennberg, P. O.; Kjaergaard, H. G. Unimolecular reactions following indoor and outdoor limonene ozonolysis. *J. Phys. Chem. A* **2021**, *125* (2), 669−680.
(34) Pagonis, D.; Algrim, L. B.; Price, D. J.; Day, D. A.; Handschy, A. V.; Stark, H.; Miller, S. L.; de Gouw, J. A.; Jimenez, J. L.; Ziemann, P. J. Autoxidation of limonene emitted in a university art museum. *Environ. Sci. Technol. Lett.* **2019**, *6* (9), 520−524.
(35) Crounse, J. D.; Nielsen, L. B.; Jørgensen, S.; Kjaergaard, H. G.; Wennberg, P. O. Autoxidation of organic compounds in the atmosphere. *J. Phys. Chem. Lett.* **2013**, *4* (20), 3513−3520.
(36) Bianchi, F.; Kurten, T.; Riva, M.; Mohr, C.; Rissanen, M. P.; Roldin, P.; Berndt, T.; Crounse, J. D.; Wennberg, P. O.; Mentel, T. F.; Wildt, J.; Junninen, H.; Jokinen, T.; Kulmala, M.; Worsnop, D. R.; Thornton, J. A.; Donahue, N.; Kjaergaard, H. G.; Ehn, M. Highly oxygenated organic molecules (hom) from gas-phase autoxidation involving peroxy radicals: A key contributor to atmospheric aerosol. *Chem. Rev.* **2019**, *119* (6), 3472−3509.
(37) Vereecken, L.; Nozière, B. H migration in peroxy radicals under atmospheric conditions. *Atmos. Chem. Phys.* **2020**, *20* (12), 7429−7458.
(38) Otkjaer, R. V.; Jakobsen, H. H.; Tram, C. M.; Kjaergaard, H. G. Calculated hydrogen shift rate constants in substituted alkyl peroxy radicals. *J. Phys. Chem. A* **2018**, *122* (43), 8665−8673.
(39) Vereecken, L.; Vu, G.; Wahner, A.; Kiendler-Scharr, A.; Nguyen, H. M. T. A structure activity relationship for ring closure reactions in unsaturated alkylperoxy radicals. *Phys. Chem. Chem. Phys.* **2021**, *23* (31), 16564−16576.
(40) Wang, Z.; Ehn, M.; Rissanen, M. P.; Garmash, O.; Quéléver, L.; Xing, L.; Monge-Palacios, M.; Rantala, P.; Donahue, N. M.; Berndt, T.; Sarathy, S. M. Efficient alkane oxidation under combustion engine and atmospheric conditions. *Commun. Chem.* **2021**, *4* (1), 1−8.
(41) Li, C.; Chen, J.; Xie, H. B.; Zhao, Y.; Xia, D.; Xu, T.; Li, X.; Qiao, X. Effects of atmospheric water on oh-initiated oxidation of organophosphate flame retardants: A dft investigation on tcpp. *Environ. Sci. Technol.* **2017**, *51* (9), 5043−5051.
(42) Fu, Z. H.; Xie, H. B.; Elm, J.; Liu, Y.; Fu, Z. Q.; Chen, J. W. Atmospheric autoxidation of organophosphate esters. *Environ. Sci. Technol.* **2022**, *56* (11), 6944−6955.
(43) Gao, Y.; Li, G.; Qin, Y.; Ji, Y.; Mai, B.; An, T. New theoretical insight into indirect photochemical transformation of fragrance nitro-musks: Mechanisms, eco-toxicity and health effects. *Environ. Int.* **2019**, *129*, 68−75.
(44) Lu, T. *Molclus program*, version 1.9.9.4. http://www.keinsci.com/research/molclus.html (accessed July 21, 2023).
(45) Glowacki, D. R.; Liang, C. H.; Morley, C.; Pilling, M. J.; Robertson, S. H. Mesmer: An open-source master equation solver for multi-energy well reactions. *J. Phys. Chem. A* **2012**, *116* (38), 9545−60.
(46) Gilbert, R. G.; Smith, S. C. *Theory of unimolecular recombination reactions*; Blackwell Scientific Publications: Carlton, Australia, 1990.
(47) Eckart, C. The penetration of a potential barrier by electrons. *Phys. Rev.* **1930**, *35* (11), 1303−1309.
(48) US Environmental Protection Agency. *User's guide for toxicity estimation software tool* (test version 4.0), 2011.
(49) Xiong, G.; Wu, Z.; Yi, J.; Fu, L.; Yang, Z.; Hsieh, C.; Yin, M.; Zeng, X.; Wu, C.; Lu, A.; Chen, X.; Hou, T.; Cao, D. Admetlab 2.0: An integrated online platform for accurate and comprehensive predictions of admet properties. *Nucleic Acids Res.* **2021**, *49* (W1), W5−W14.
(50) Mayo-Bean, K.; Moran-Bruce, K.; Meylan, W.; Ranslow, P.; Lock, M.; Nabholz, J. V.; Runnen, J. V.; Cassidy, L. M.; Tunkel, J. *Methodology document for the ecological structure−activity relationship model (ecosar) class program*, version 2.0; Office of Pollution Prevention Toxics, US Environmental Protection Agency: Washington DC, 2017.
(51) Qiao, L.; Gao, L.; Huang, D.; Liu, Y.; Xu, C.; Li, D.; Zheng, M. Screening of toxcast chemicals responsible for human adverse outcomes with exposure to ambient air. *Environ. Sci. Technol.* **2022**, *56* (11), 7288−7297.
(52) Guo, Z.; Chen, X.; Wu, D.; Huo, Y.; Cheng, A.; Liu, Y.; Li, Q.; Chen, J. Higher toxicity of gaseous organics relative to particulate matters emitted from typical cooking processes. *Environ. Sci. Technol.* **2023**, *57* (44), 17022−17031.
(53) Orlando, J. J.; Tyndall, G. S. Laboratory studies of organic peroxy radical chemistry: An overview with emphasis on recent issues of atmospheric significance. *Chem. Soc. Rev.* **2012**, *41*, 6294−6317.
(54) Kroll, J. H.; Seinfeld, J. H. Chemistry of secondary organic aerosol: Formation and evolution of low-volatility organics in the atmosphere. *Atmos. Environ.* **2008**, *42*, 3593−3624.
(55) Jenkin, M. E.; Valorso, R.; Aumont, B.; Rickard, A. R. Estimation of rate coefficients and branching ratios for reactions of

organic peroxy radicals for use in automated mechanism construction. *Atmos. Chem. Phys.* **2019**, *19* (11), 7691−7717.
(56) Weschler, C. J.; Shields, H. C.; Naik, D. V. Indoor chemistry involving o3, no, and no2 as evidenced by 14 months of measurements at a site in southern california. *Environ. Sci. Technol.* **1994**, *28* (12), 2120−2132.
(57) Fu, Z. H.; Xie, H. B.; Elm, J.; Guo, X. R.; Fu, Z. Q.; Chen, J. W. Formation of low-volatile products and unexpected high formaldehyde yield from the atmospheric oxidation of methylsiloxanes. *Environ. Sci. Technol.* **2020**, *54* (12), 7136−7145.
(58) Pagonis, D.; Price, D. J.; Algrim, L. B.; Day, D. A.; Handschy, A. V.; Stark, H.; Miller, S. L.; de Gouw, J.; Jimenez, J. L.; Ziemann, P. J. Time-resolved measurements of indoor chemical emissions, deposition, and reactions in a university art museum. *Environ. Sci. Technol.* **2019**, *53* (9), 4794−4802.
(59) Liu, S.; Li, R.; Wild, R. J.; Warneke, C.; de Gouw, J. A.; Brown, S. S.; Miller, S. L.; Luongo, J. C.; Jimenez, J. L.; Ziemann, P. J. Contribution of human-related sources to indoor volatile organic compounds in a university classroom. *Indoor air* **2016**, *26* (6), 925−938.
(60) Mendez, M.; Amedro, D.; Blond, N.; Hauglustaine, D. A.; Blondeau, P.; Afif, C.; Fittschen, C.; Schoemaecker, C. Identification of the major hox radical pathways in an indoor air environment. *Indoor air* **2017**, *27* (2), 434−442.
(61) Atkinson, R.; Arey, J. Atmospheric degradation of volatile organic compounds. *Chem. Rev.* **2003**, *103*, 4605−4638.
(62) Boyd, A. A.; Flaud, P.-M.; Daugey, N.; Lesclaux, R. Rate constants for ro2 + ho2 reactions measured under a large excess of ho2. *J. Phys. Chem. A* **2003**, *107*, 818−821.
(63) Piletic, I. R.; Kleindienst, T. E. Rates and yields of unimolecular reactions producing highly oxidized peroxy radicals in the oh-induced autoxidation of α-pinene, β-pinene, and limonene. *J. Phys. Chem. A* **2022**, *126* (1), 88−100.
(64) Gilmore, K.; Mohamed, R. K.; Alabugin, I. V. The baldwin rules: Revised and extended. *Wiley Interdiscip. Rev.: Comput. Mol. Sci.* **2016**, *6* (5), 487−514.
(65) Nozière, B.; Vereecken, L. Direct observation of aliphatic peroxy radical autoxidation and water effects: An experimental and theoretical study. *Angew. Chem., Int. Ed.* **2019**, *58* (39), 13976−13982.
(66) Liu, L.; Zhang, X.; Li, Z.; Zhang, Y.; Ge, M. Gas-phase hydration of glyoxylic acid: Kinetics and atmospheric implications. *Chemosphere* **2017**, *186*, 430−437.
(67) Donahue, N. M.; Robinson, A. L.; Stanier, C. O.; Pandis, S. N. Coupled partitioning, dilution, and chemical aging of semivolatile organics. *Environ. Sci. Technol.* **2006**, *40* (8), 2635−2643.
(68) Paulot, F.; Crounse, J. D.; Kjaergaard, H. G.; Kürten, A.; St. Clair, J. M.; Seinfeld, J. H.; Wennberg, P. O. Unexpected epoxide formation in the gas-phase photooxidation of isoprene. *Science* **2009**, *325* (5941), 730−733.
(69) Fu, Z.; Ma, F.; Liu, Y.; Yan, C.; Huang, D.; Chen, J.; Elm, J.; Li, Y.; Ding, A.; Pichelstorfer, L.; Xie, H.-B.; Nie, W.; Francisco, J. S.; Zhou, P. An overlooked oxidation mechanism of toluene: Computational predictions and experimental validations. *Chem. Sci.* **2023**, *14* (45), 13050−13059.
(70) Gkatzelis, G. I.; Papanastasiou, D. K.; Karydis, V. A.; Hohaus, T.; Liu, Y.; Schmitt, S. H.; Schlag, P.; Fuchs, H.; Novelli, A.; Chen, Q.; Cheng, X.; Broch, S.; Dong, H.; Holland, F.; Li, X.; Liu, Y.; Ma, X.; Reimer, D.; Rohrer, F.; Shao, M.; Tan, Z.; Taraborrelli, D.; Tillmann, R.; Wang, H.; Wang, Y.; Wu, Y.; Wu, Z.; Zeng, L.; Zheng, J.; Hu, M.; Lu, K.; Hofzumahaus, A.; Zhang, Y.; Wahner, A.; Kiendler-Scharr, A. Uptake of water-soluble gas-phase oxidation products drives organic particulate pollution in beijing. *Geophys. Res. Lett.* **2021**, DOI: 10.1029/2020GL091351.
(71) Guo, S.; Hu, M.; Guo, Q.; Zhang, X.; Zheng, M.; Zheng, J.; Chang, C. C.; Schauer, J. J.; Zhang, R. Primary sources and secondary formation of organic aerosols in beijing, china. *Environ. Sci. Technol.* **2012**, *46* (18), 9846−53.
(72) Wong, J. P. S.; Carslaw, N.; Zhao, R.; Zhou, S.; Abbatt, J. P. D. Observations and impacts of bleach washing on indoor chlorine chemistry. *Indoor air* **2017**, *27* (6), 1082−1090.
(73) Weschler, C. J.; Carslaw, N. Indoor chemistry. *Environ. Sci. Technol.* **2018**, *52* (5), 2419−2428.